Purinergic $P2Y_{14}$ receptor modulates stress-induced hematopoietic stem/progenitor cell senescence

Joonseok Cho,[1,2] Rushdia Yusuf,[3,4,5] Sungho Kook,[1,2,6] Eyal Attar,[3,4,5] Dongjun Lee,[3,4,5] Baehang Park,[1,2] Tao Cheng,[7] David T. Scadden,[3,4,5] and Byeong Chel Lee[1,2]

[1]University of Pittsburgh Cancer Institute and [2]Department of Medicine, Division of Hematology and Oncology, University of Pittsburgh School of Medicine, Pittsburgh, Pennsylvania, USA. [3]Center for Regenerative Medicine and Cancer Center, Massachusetts General Hospital, Boston, Massachusetts, USA. [4]Harvard Stem Cell Institute and [5]Department of Stem Cell and Regenerative Biology, Harvard University, Cambridge, Massachusetts, USA. [6]Institute for Molecular Biology and Genetics, Chonbuk National University, Jeonju, Republic of Korea. [7]State Key Laboratory of Experimental Hematology, Institute of Hematology and Blood Disease Hospital, Center for Stem Cell Medicine, Chinese Academy of Medical Sciences and Peking Union Medical College, Tianjin, China.

Purinergic receptors of the P2Y family are G protein–coupled surface receptors that respond to extracellular nucleotides and can mediate responses to local cell damage. P2Y-dependent signaling contributes to thrombotic and/or inflammatory consequences of tissue injury by altering platelet and endothelial activation and immune cell phagocytosis. Here, we have demonstrated that $P2Y_{14}$ modifies cell senescence and cell death in response to tissue stress, thereby enabling preservation of hematopoietic stem/progenitor cell function. In mice, $P2Y_{14}$ deficiency had no demonstrable effect under homeostatic conditions; however, radiation stress, aging, sequential exposure to chemotherapy, and serial bone marrow transplantation increased senescence in animals lacking $P2Y_{14}$. Enhanced senescence coincided with increased ROS, elevated $p16^{INK4a}$ expression, and hypophosphorylated Rb and was inhibited by treatment with a ROS scavenger or inhibition of p38/MAPK and JNK. Treatment of WT cells with pertussis toxin recapitulated the $P2Y_{14}$ phenotype, suggesting that $P2Y_{14}$ mediates antisenescence effects through Gi/o protein–dependent pathways. Primitive hematopoietic cells lacking $P2Y_{14}$ were compromised in their ability to restore hematopoiesis in irradiated mice. Together, these data indicate that $P2Y_{14}$ on stem/progenitor cells of the hematopoietic system inhibits cell senescence by monitoring and responding to the extracellular manifestations of tissue stress and suggest that $P2Y_{14}$-mediated responses prevent the premature decline of regenerative capacity after injury.

Introduction

Organisms inevitably encounter a variety of stresses during their lifetimes, including radiation, oxidation, and infection. The nature and efficiency of the response to stress is a fundamental determinant of an organism's fitness, with dysfunctional responses serving as putative instigators of malignancy and degenerative diseases.

Nucleotides, long known as metabolic substrates, are now also recognized as key extracellular messengers that regulate diverse aspects of homeostasis in various pathophysiological conditions (1). Stress causes purines and pyrimidines to accumulate in the extracellular space, which alerts the cell to danger through interaction with purinergic receptors (2). They have been shown to serve as a "find me signal" for macrophages to detect and engulf apoptotic cells (3).

Purinergic receptors are classified into P1 and P2 receptors, based on their ligand binding and function (4). P2 receptors are further subdivided into the P2X (ion channel) and the P2Y (G protein coupled) receptor subtypes. P2 receptors are detected not only in mammalian species, but also in chicken (5) and *Xenopus* (6). The homology between P2 receptors in the amino acid sequence is relatively low (19%–55% sequence identity at the amino acid level) (7, 8).

The role of P2 receptors as regulators of hematopoiesis has been documented (9, 10), but the underlying mechanisms by which purinergic receptors exert their effects in hematopoietic cells have not been studied in detail. Hematopoietic tissues are among the most sensitive to ionizing radiation–induced (IR-induced) damage. While IR can result in either apoptosis or senescence, it has been suggested by some that stress-induced premature senescence (SIPS) may predominate over apoptosis (11, 12). It has also been reported that IR selectively induces senescence in HSCs (13). HSC senescence represents an irreversible loss of proliferation capacity and could compromise HSC ability to react to environmental stress to maintain their delicate homeostatic balance. How stem cells respond or adapt to stress has central implications for regenerative medicine.

We previously constructed a subtractive cDNA library to enrich for differentially expressed transcripts from adult human BM-derived hematopoietic stem progenitor cell (HSPC) populations (G0, $CD34^+CD38^-$) (14). Among the genes isolated from the subtractive cDNA library, *P2RY14*, a 7-transmembrane G protein–coupled purinergic receptor (7TM GPCR), shows highly restrictive expression in human HSPC, and its expression is associated with cell-cycle dormancy.

Herein, we provide evidence demonstrating that $P2Y_{14}$ expression is indispensable for maintaining homeostasis in HSPCs and embryos under stress and define it as a receptor mediator of cell senescence.

Authorship note: Joonseok Cho, Rushdia Yusuf, and Sungho Kook contributed equally to this work.

Conflict of interest: The authors have declared that no conflict of interest exists.

Citation for this article: *J Clin Invest.* 2014;124(7):3159–3171. doi:10.1172/JCI61636.

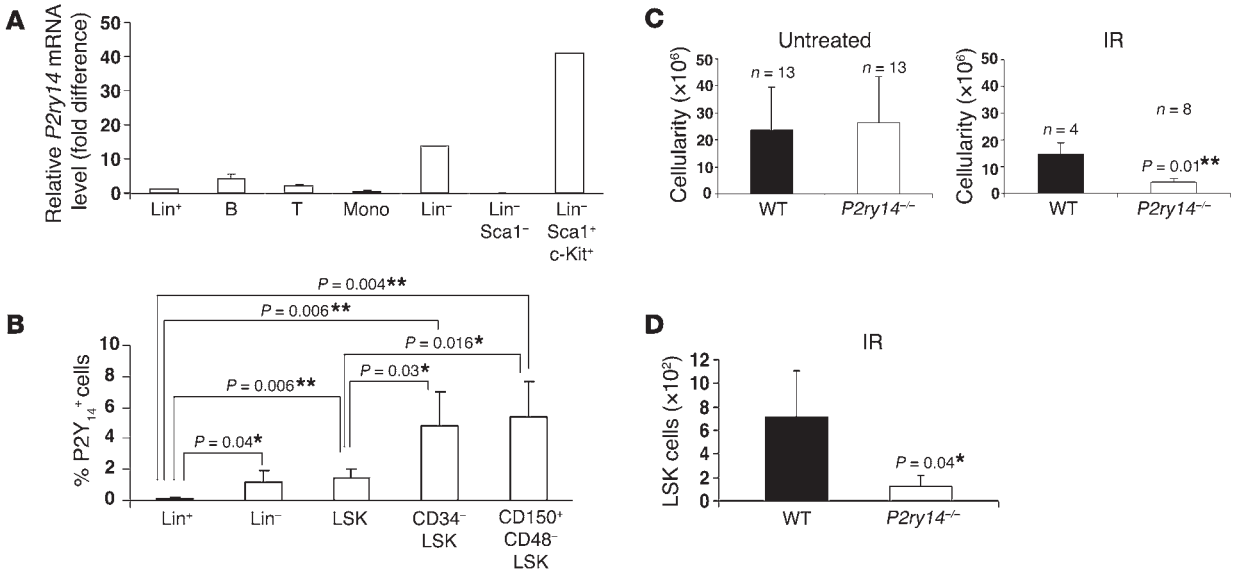

Figure 1

$P2Y_{14}$ deficiency increases the susceptibility of HSPCs to radiation stress. (**A**) Q-PCR analysis of *P2ry14* mRNA: mRNA from BM cells bearing the indicated phenotype was analyzed by Q-PCR. The expression was normalized to GAPDH. The expression level in lineage positive (Lin^+) cells was arbitrarily set to 1. Q-PCR was done in duplicate. B, B cells ($B220^+$); T, T cells ($CD3^+$); mono, monocytes ($CD11b^+$). (**B**) Cells were gated as indicated, and the expression of $P2Y_{14}$ was measured within the gates. The percentage of $P2Y_{14}$-expressing ($P2Y_{14}^+$) cells in indicated compartments is plotted on the *y* axis. The data are representative of at least 3 independent experiments, each with 3 mice per group. (**C**) Mice of the indicated genotypes were exposed to TBI (3 × 5 Gy). Recipients were allowed to recover for 15 days before the next dose was administered. The number of BM cells was counted within the marrow of femur and tibia. (**D**) The number of LSK cells was measured after TBI (3 × 5 Gy TBI, 15 days apart). Data show representative mice of at least 6 animals analyzed per group. Statistical analyses were carried out using 1-tailed Student's *t* test (**C** and **D**) and 2-tailed Student's *t* test (**B**). $^*P < 0.05$; $^{**}P < 0.01$.

Results

$P2Y_{14}$ deficiency renders HSPCs more susceptible to radiation-induced senescence and cell death. Mice deficient in *P2ry14* were generated by the targeted gene deletion of the sequences encoding TM2–TM7 as described (15). Absence of $P2Y_{14}$ in KO (*P2ry14*$^{-/-}$) mice was confirmed by genotyping, quantitative RT-PCR (Q–RT-PCR), and flow cytometry analysis (Supplemental Figure 1; supplemental material available online with this article; doi:10.1172/JCI61636DS1). $P2Y_{14}$ KO mice displayed no obvious phenotypic abnormality when compared with their heterozygous (HT) (*P2ry14*$^{+/-}$) and WT (*P2ry14*$^{+/+}$) littermates. Breeding of $P2Y_{14}$ HT mice resulted in approximately the expected Mendelian ratios of offspring, indicating that the mutation is not associated with embryonic or neonatal lethality (16). Medians of wbc count, rbc count, platelet (PLT) count, and hemoglobin (HGB) count were comparable between $P2Y_{14}$ KO and WT mice (Supplemental Figure 2). Similarly, BM common lymphoid progenitors (CLPs), common myeloid progenitors (CMPs), granulocyte-monocyte progenitors (GMPs), and megakaryocyte-erythrocyte progenitors (MEPs) were not significantly different (data not shown). Modest increases in multipotent progenitors ($CD34^-$, Lin^-, $Sca\text{-}1^+$, $c\text{-}Kit^+$) (CD34-LSK) (1.8- to 2.5-fold, $P = 0.04$) and LSK (~1.3 fold, $P = 0.006$), but no statistically significant changes in $CD150^+CD48^-$ LSK cells ($P = 0.17$) were observed in KO compared with WT littermates (Supplemental Figure 3). Thus, $P2Y_{14}$ KO mice have seemingly normal hematopoiesis under steady state conditions.

P2ry14 is detected in various types of hematopoietic cells. However, *P2ry14* expression is particularly prominent in murine LSK cells (Figure 1A), consistent with our prior findings in the human HSPCs (14). Thus, the expression of *P2ry14* preferentially occurs in HSPCs in both mice and humans.

We next assessed the percentage of $P2Y_{14}$-expressing cells ($P2Y_{14}^+$) in previously defined HSPC populations. The specificity of the $P2Y_{14}$ antibody was confirmed by the lack of $P2Y_{14}$ expression in $P2Y_{14}$ KO Lin^- cells (Supplemental Figure 1). Enriching primitive HSCs using previously known phenotypic markers (e.g., $CD34^-$ LSK or $CD150^+CD48^-$ LSK) increased the percentage of $P2Y_{14}$-expressing cells (Figure 1B). However, $P2Y_{14}^+$ cells represented a relatively small proportion of cells within previously defined HSCs, raising the possibility that $P2Y_{14}$ expression may define a functionally unique HSPC subset.

Purinergic receptors, including $P2Y_{14}$, are hypothesized to play a role in modulating the stress response. Evaluation of $P2Y_{14}$ expression demonstrated increased levels in hematopoietic cells in association with various types of stress. (Supplemental Figure 4). These data reinforce the potential link of $P2Y_{14}$ to a stress response (17), which we investigated further.

Hematopoietic cells are extremely vulnerable to genotoxic stress–induced cell injury. We therefore assessed whether $P2Y_{14}$ deficiency modulates the susceptibility of hematopoietic cells to radiation stress. Since different doses of IR can produce different biological consequences, we examined the effects of low (3 Gy), medium (6 Gy), and high (8 Gy) doses of radiation on the IR-induced cell injury. 3 Gy total body irradiation (TBI) did not cause a statistically significant difference in IR-induced cell death between WT and KO LSK cells (Supplemental Figure 5). At doses of greater than 8 Gy,

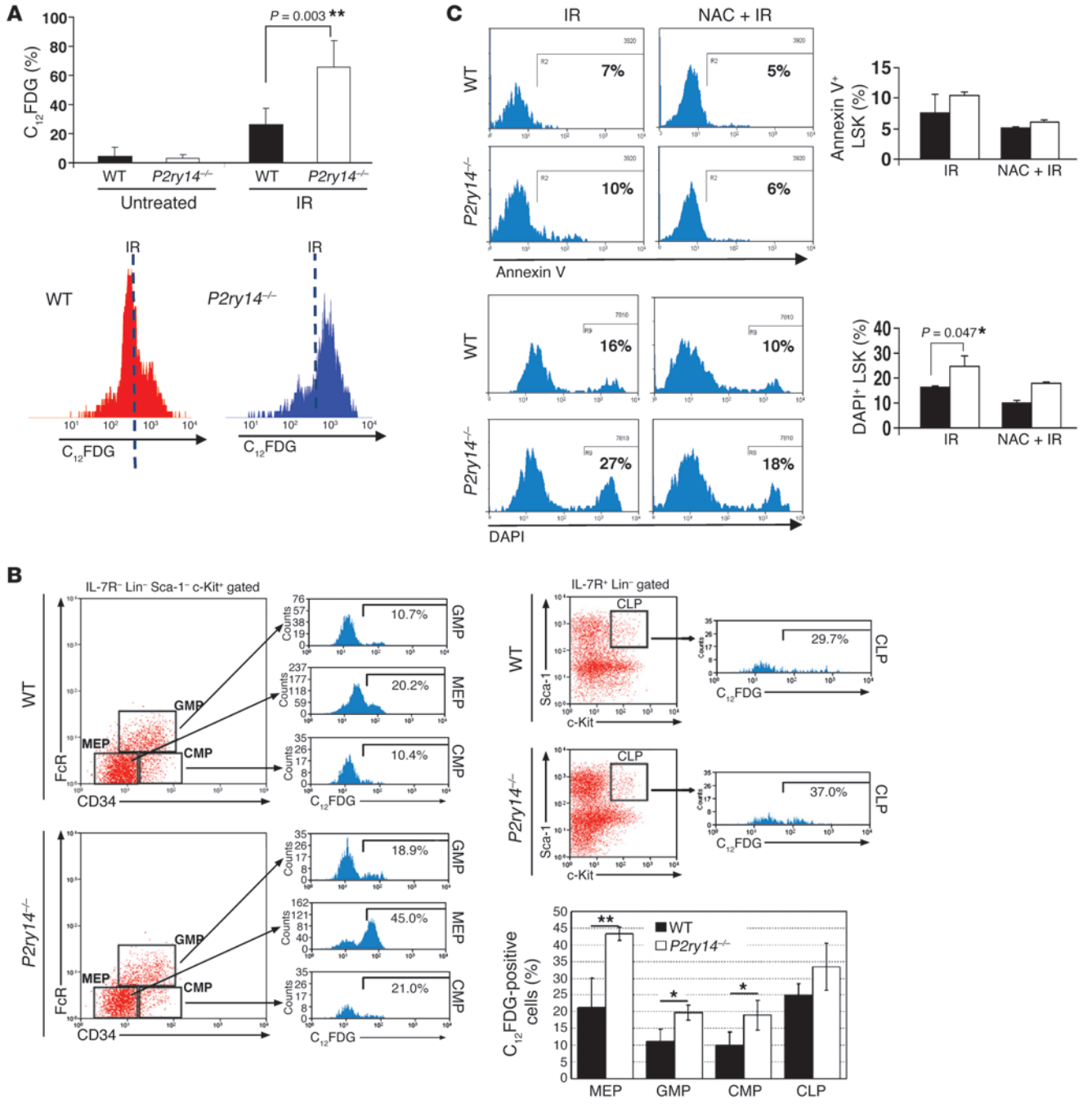

Figure 2

$P2Y_{14}$ deficiency increases the susceptibility of HSPCs to radiation-induced senescence and cell death. (**A**) Mice of the indicated genotypes were exposed to TBI (6 Gy). SA–β-gal activity was determined using C_{12}FDG. Percentage of SA–β-gal–positive LSK population (upper) is expressed as mean ± SD. The data are representative of 6 mice per group. Representative histograms of SA–β-gal staining in gated LSK cell (lower). (**B**) BM cells from irradiated *P2ry14*$^{-/-}$ and WT mice (6 Gy TBI) were stained with the indicated antibodies. Lineage-committed progenitor cells were gated based on defined phenotypic criteria, and cellular senescence was measured in each gated population. Numbers indicate the percentage of $C_{12}FDG^+$ cells in the indicated gates. The accompanying graph shows the mean percentage of $C_{12}FDG^+$ cells (± SD) in each gated population (n = 5/genotype). (**C**) Cell death analysis in gated LSK cells. Cell death was measured by quantification of annexin V$^+$ or DAPI$^+$ (gated on annexin V$^-$) cells 8 hours after TBI (6 Gy). The data are representative of 2 independent experiments each, with BM cells pooled from 2 mice per group. NAC (100 mg/kg) was injected s.c. 4 hours before and 2 hours after TBI. Representative flow cytometric analysis of annexin V$^+$ (upper left) and DAPI$^+$, annexin V$^-$ (lower left) LSK cells is shown. Percentages of gated cell populations are indicated. Statistical analyses were carried out using 1-tailed Student's t test (**C**) and 2-tailed Student's t test (**A** and **B**). *$P < 0.05$; **$P < 0.01$.

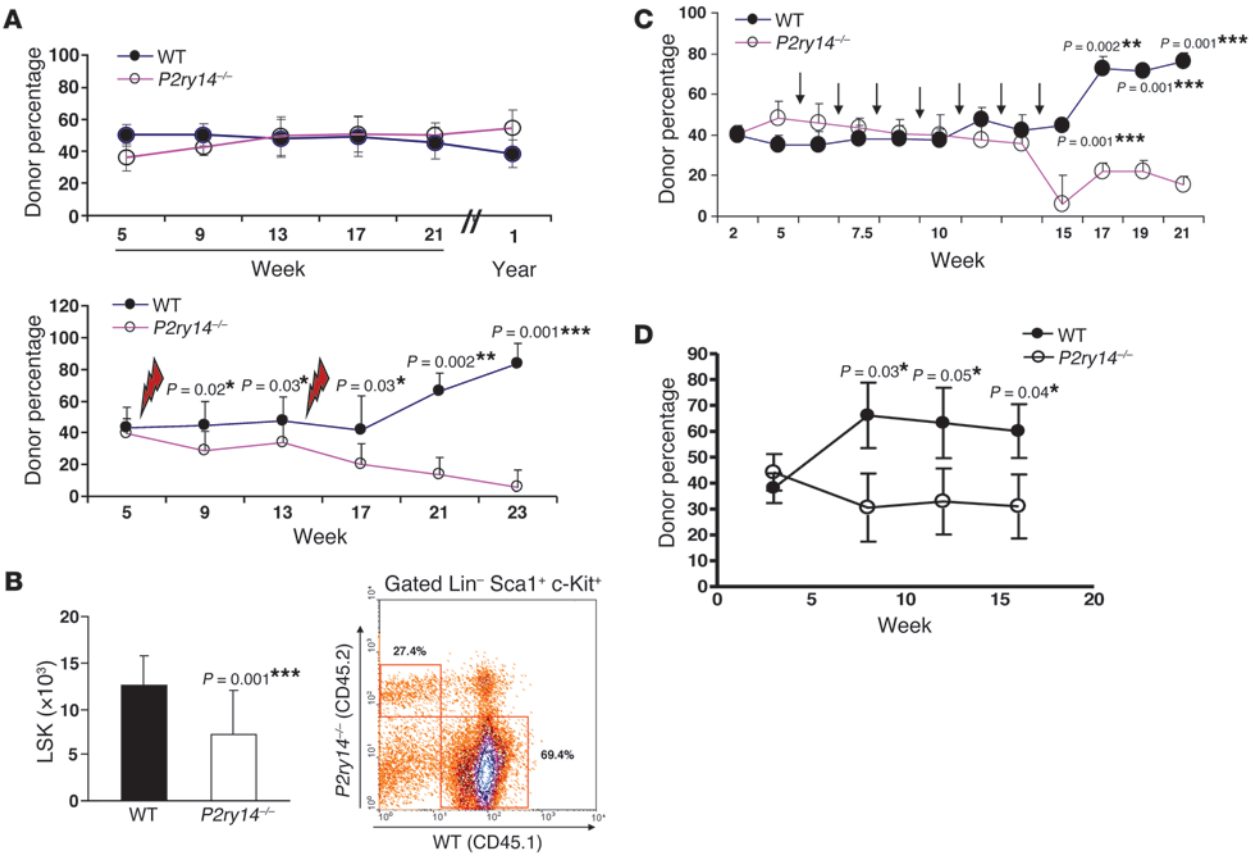

Figure 3

$P2Y_{14}$ deficiency increases the susceptibility of HSPCs to various hematological stresses. (**A**) A mixture of BM cells from *P2ry14*$^{-/-}$ (CD45.2) and congenic WT (CD45.1) mice were transplanted into recipients (CD45.1.2, $n = 16$) as described in Methods. The *x* axis denotes the number of weeks after transplantation. Upper panel: untreated mice ($n = 6$); lower panel; 5 weeks after transplantation, a group of recipients ($n = 10$) were irradiated (6 Gy TBI) and then the contributions of WT (CD45.1) and *P2ry14*$^{-/-}$ (CD45.2) cells to the recipients' blood were measured. Lightning bolts mark the timing of IR. (**B**) BM cells from *P2ry14*$^{-/-}$ and WT mice were transplanted as described in **A**. Eight to nine months after transplantation, recipients ($n = 8$) were irradiated (6 Gy) and the frequency of WT and *P2ry14*$^{-/-}$ derived LSK cells in recipients' BM was assessed at 5 weeks after IR (right). The accompanying graph (left) shows the absolute numbers of LSK cells. (**C**) WT and *P2ry14*$^{-/-}$ BM cells were transplanted as described in **A**. Five weeks after transplantation, recipients ($n = 6$) were treated with 5-FU (150 mg/kg). Recipients were allowed to recover for 9 days before the next dose was administered. The *x* axis denotes the number of weeks after transplantation. Arrows mark the timing of injection. Ratio of WT and *P2ry14*$^{-/-}$ cells in recipients' blood was determined 7 days after each 5-FU injection. (**D**) Contribution of WT and *P2ry14*$^{-/-}$ cells after secondary transplantation ($n = 4$/genotype). The *x* axis denotes the number of weeks after transplantation. Statistical analyses were carried out using 1-tailed Student's *t* test (**B**) and 2-tailed Student's *t* test (**A**, **C**, and **D**). $^*P < 0.05$; $^{**}P < 0.01$; $^{***}P < 0.001$.

only a very small number of HSPCs were alive (data not shown), making further analysis difficult. At 5 to 6 Gy TBI, a distinct effect on $P2Y_{14}$-deficient LSKs compared with WT counterparts was noted (Supplemental Figure 5). Others have documented that TBI at those doses rarely resulted in animal death, but induced both acute and long-term hematopoietic dysfunction (13).

On the basis of these results, $P2Y_{14}$ KO and WT littermate mice were exposed to 5 Gy TBI, and the number of nucleated cells in the BM was measured. As expected, WT mice showed a reduction of BM cell numbers in response to radiation. However, a more severe reduction was observed in $P2Y_{14}$ KO mice (Figure 1C). We then examined whether $P2Y_{14}$ expression in stem/progenitor cells played a role in modulating their susceptibility to radiation. As shown in Figure 1D, $P2Y_{14}$ KO LSK cells were more susceptible to IR stress than WT counterparts and showed a considerably lower LSK cell number (Figure 1D) and frequency (WT vs. KO: 1.92% ± 0.36% vs. 1.08% ± 0.55%, $P = 0.037$). Preferential decrease of the $P2Y_{14}$ KO LSK cells could be the result of increased susceptibility to IR-induced senescence or cell death or both. Since sublethal radiation has been reported to selectively induce HSC senescence (13), we focused on this cell process. LSK cells lacking $P2Y_{14}$ showed a markedly increased level of senescence-associated β-gal (SA-β-gal) activity ($P = 0.003$) (Figure 2A) consistent with increased susceptibility to IR-induced senescence. Differential sensitivity to IR-induced senescence was observed in multipotent as well as lineage-committed progenitor cells lacking $P2Y_{14}$, including CLP, CMP, GMP, and MEP (Figure 2B). Radiation induces both apoptotic and nonapoptotic cell death (18). There was a modest trend toward increased IR-induced apoptosis (annexin V$^+$) in $P2Y_{14}$ KO LSK cells (Figure 2C). However, a higher rate of annexin V$^-$, DAPI$^+$ cells ($P = 0.047$) was detected (Figure 2C), suggesting that $P2Y_{14}$ KO HSPCs may die primarily through nonapoptotic rather than apoptotic pathways.

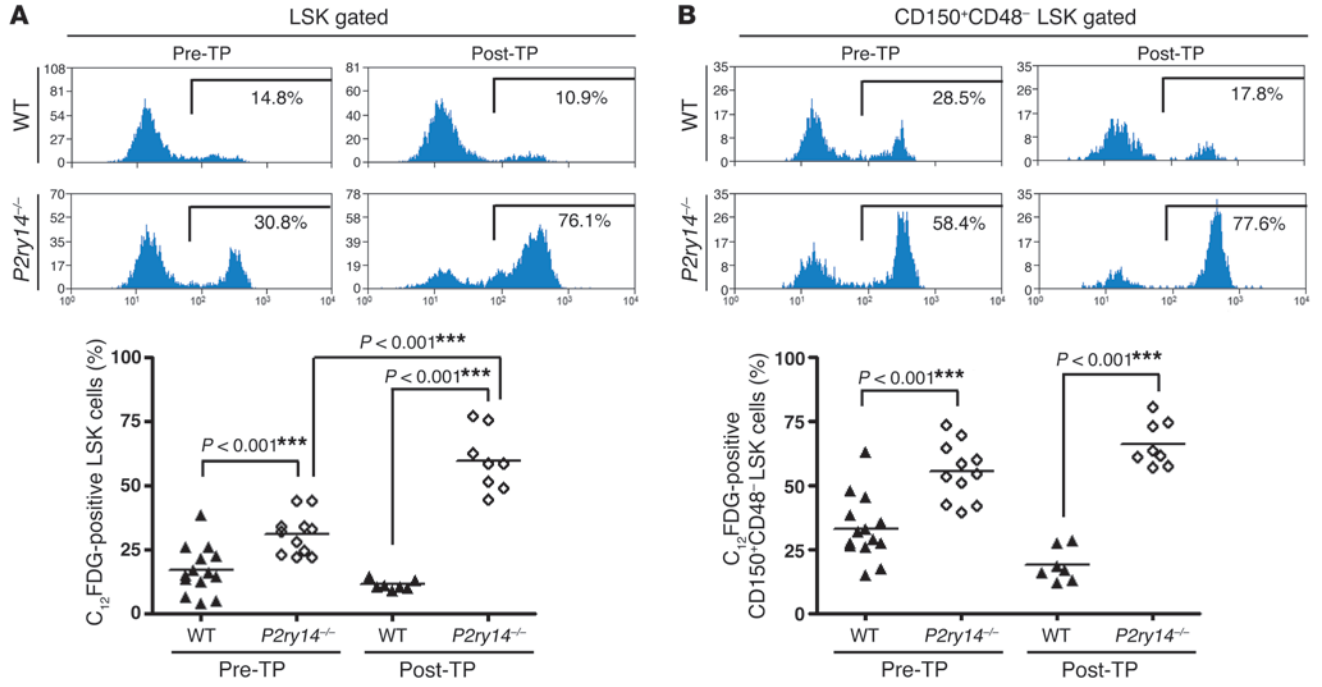

Figure 4

Impact of $P2Y_{14}$ deficiency on HSPC senescence during the natural aging process. (**A** and **B**) KO and WT mice were maintained in a pathogen-free environment for 90–100 weeks before collection of BM cells for senescence analysis. Representative flow cytometric analyses of C_{12}FDG in LSK (**A**) and $CD150^+CD48^-$ LSK (**B**) cells from WT and *P2ry14*$^{-/-}$ mice are shown. Percentages of gated cell populations are indicated. BM cells isolated from 90- to 100-week-old WT and KO mice (CD45.2) were further transplanted into lethally irradiated recipient mice (CD45.1.2). Donor-derived $CD45.2^+$ LSK (**A**, Post-TP) and $CD45.2^+CD150^+CD48^-$ LSK (**B**, Post-TP) cells were analyzed for SA–β-gal–positive cells using C_{12}FDG. The accompanying graphs show the mean percentage of C_{12}FDG-positive LSK (**A**) and $CD150^+CD48^-$ LSK (**B**) cells. The 2-tailed Student's *t*-test was used. Pre-TP, pretransplantation; post-TP, post-transplantation. ***$P < 0.001$.

$P2Y_{14}$ deficiency compromises the ability of HSPCs to respond to hematological stress. To assess whether WT-derived cells have a competitive advantage over $P2Y_{14}$ KO–derived cells under stress, we performed competitive repopulation assays. $P2Y_{14}$ mice were backcrossed 8 times with C57BL/6J (B6) mice, which made them more than 99% genetically identical to B6 mice. Therefore, BM cells from CD45.1 congenic strains of B6 were used as WT control (B6, CD45.1). When $P2Y_{14}$ KO (B6, CD45.2) and WT BM (B6, CD45.1) cells were cotransplanted into lethally irradiated WT recipients (CD45.1.2), there was a similar contribution from KO and WT cells in recipient mice 5 weeks after transplantation, and this ratio remained constant for at least 1 year (Figure 3A). However, when these recipient animals were irradiated, $P2Y_{14}$ KO–derived cells (CD45.2) showed a progressive decline in their competitive capacity against WT-derived cells (CD45.1) (Figure 3A). These changes became more prominent as the recipients were treated with a second round of IR (Figure 3A).

We then asked whether this preferential reduction of $P2Y_{14}$ KO–derived cells within the WT microenvironment was due to higher sensitivity of $P2Y_{14}$ KO HSPCs to radiation. Recipient mice undergoing IR treatment showed a marked difference in the frequency of donor-derived LSK cells in their BM, displaying a preferential depletion of $P2Y_{14}$ KO–derived LSK cells (KO-derived LSK vs. WT-derived LSK; 27% vs. 69%) (Figure 3B). These data suggest a hematopoietic cell-autonomous basis for the differential sensitivity to IR.

Multiple doses of cytotoxic chemotherapy are generally used in cancer patients, and we evaluated whether $P2Y_{14}$ expression affected resistance to repetitive 5-fluorouracil (5-FU) treatment. Recipient animals were treated with 5-FU and allowed to recover for 9 days before the next dose was administered. The degree of contribution by $P2Y_{14}$ KO– and WT-derived cells was approximately equal until the sixth injection (Figure 3C). However, the level of $P2Y_{14}$ KO–derived cells was dramatically reduced after the seventh injection and remained low thereafter (Figure 3C).

If the observed phenotypic changes in $P2Y_{14}$ KO mice are due to increased susceptibility of $P2Y_{14}$ KO HSPCs to stress, one would expect that $P2Y_{14}$ KO HSPCs would display a repopulating disadvantage in the setting of serial transplantation, since this procedure also imposes extreme stress on the HSCs (19). In the first round of transplantation, equal contributions from the WT versus $P2Y_{14}$ KO cells were observed in recipients' peripheral blood (PB), similar to that shown in Figure 3A. However, WT cells began to show a competitive repopulating advantage over $P2Y_{14}$ KO cells when they were subjected to secondary transplantation (Figure 3D).

Taken together, these results indicate that $P2Y_{14}$ KO HSPCs are functionally compromised in their ability to cope with multiple types of hematological stress.

$P2Y_{14}$ deficiency renders HSPCs more susceptible to senescence during aging. $P2Y_{14}$ KO mice showed no apparent outward signs of accelerated aging at up to 2 years of age (data not shown). Unless the mice were exposed to stress, no obvious differences in senescence and cell death were observed between the $P2Y_{14}$ KO and WT HSPCs at a relatively young age (>4–6 months old, see Figure 2). However, $P2Y_{14}$-deficient LSK (Figure 4A) and $CD150^+CD48^-$ LSK (Figure 4B)

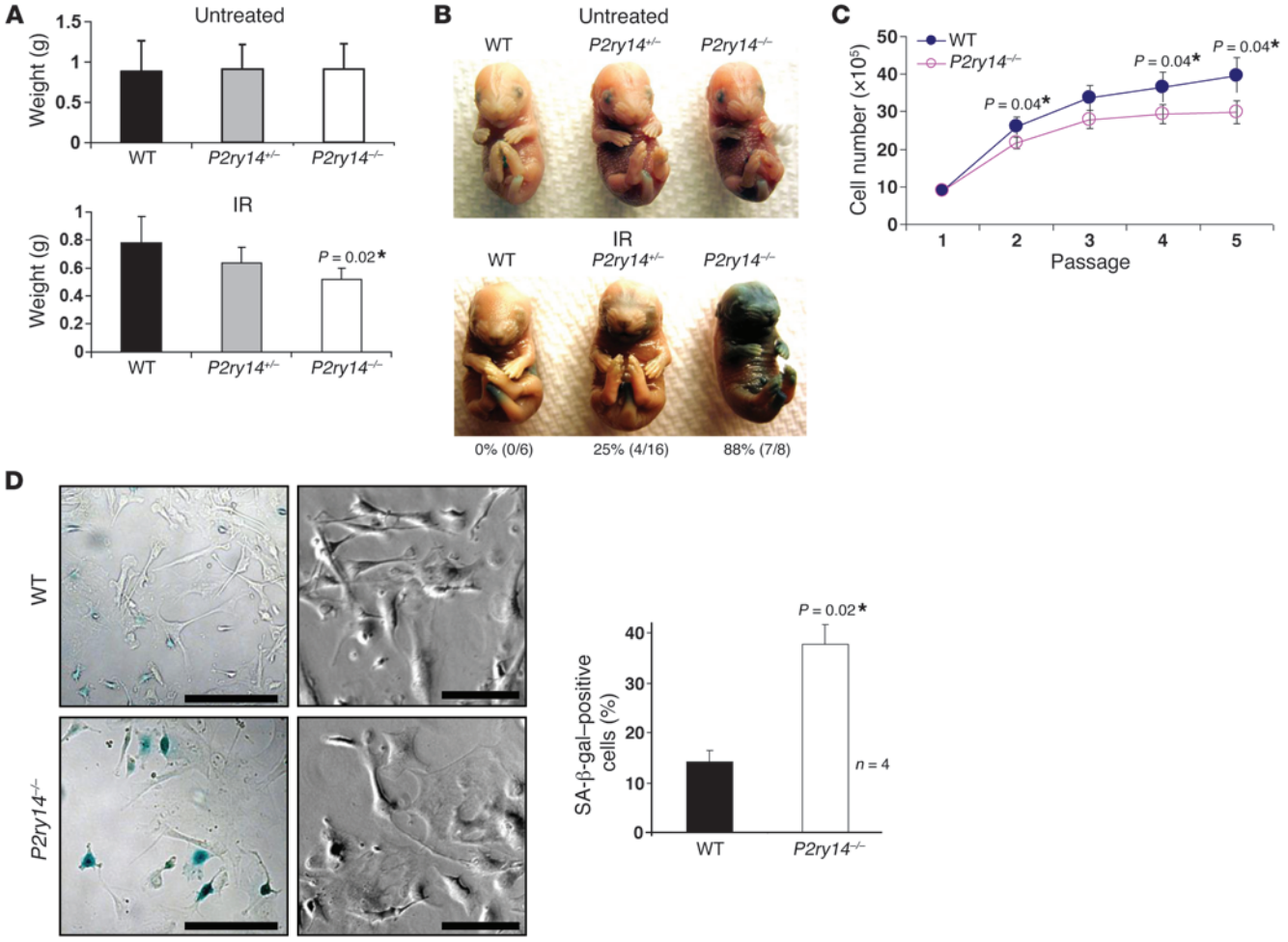

Figure 5

Impact of $P2Y_{14}$ deficiency on radiation-induced senescence during embryonic development. (**A** and **B**) HT mice were mated, and pregnant female mice were either untreated or treated (IR) with single TBI at a dose of 1.5 Gy on day 11.5 of gestation. The yolk sac was dissected and used as a source of DNA for genotyping. (**A**) E18.5 embryos isolated from untreated (upper) and treated (1.5 Gy TBI, lower) pregnant dams were weighed. (**B**) Representative images of SA–β-gal stained embryos are shown. Numbers below the bottom panel denote percentage of SA–β-gal positive embryos for each indicated genotype. Numbers in parentheses indicate the number of positively stained embryos/total number of embryo stained. (**C**) MEFs were prepared from E12.5–E13.5 *P2ry14*$^{-/-}$ and WT embryos. Cell numbers were determined at each passage prior to redilution. The 2-tailed Student's *t* test was used. (**D**) SA–β-gal staining of WT and *P2ry14*$^{-/-}$ MEF cells: MEF cells at passage 4 were subjected to SA–β-gal staining (left). The number of SA–β-gal–positive cells was counted, and the percentage of SA– β-gal positive cells is shown on the *y* axis (right). At least 50 cells from 3 random fields were counted. The 2-tailed Student's *t* test was used. Note that *P2ry14*$^{-/-}$ MEFs developed a senescence-like morphology, such as a large and flattened morphology (left). Data are representative of 4 independent experiments. Scale bars: 50 μm (left panels); 20 μm (right panels). *$P < 0.05$.

cells displayed significantly higher levels of SA–β-gal activity compared with WT counterparts at 2 years of age. Differences were even more obvious when the BM cells from the old mice were further transplanted into recipient animals (Figure 4, A and B). Collectively, these findings suggest the possibility that $P2Y_{14}$ deficiency may also affect HSPC senescence in the process of aging.

$P2Y_{14}$ is implicated in genotoxic stress responses during embryonic development. Many purinergic receptors are abundantly expressed during embryonic development (20). $P2Y_{14}$ is also expressed at a high level in the yolk sac and aorta-gonad-mesonephros (AGM) at E10.5 (our unpublished observations). The developing embryo is exceptionally sensitive to damage from radiation, and we thus sought to determine whether $P2Y_{14}$ deficiency affects the embryo's ability to cope with radiation stress. Pregnant females (HT mating) were exposed to 1.5 Gy TBI because doses higher than 1.9 Gy dramatically increased fetal death, as we and others observed (21, 22). On the 18th to 19th day of gestation, pregnant dams were autopsied and fetuses were examined for external abnormalities. Exposing pregnant dams to 1.5 Gy TBI did not result in a significant prenatal death or teratogenic malformation, and the genotype ratio of viable embryos was close to the expected Mendelian ratio. These data suggest that $P2Y_{14}$ deficiency did not cause preferential post-implantation loss of $P2Y_{14}$ KO embryos, at least at this dose of radiation. Of note, however, following prenatal radiation exposure, mean body weights of $P2Y_{14}$ KO embryos were significantly lower ($P = 0.02$) than their HT or WT littermates (Figure 5A). The weight

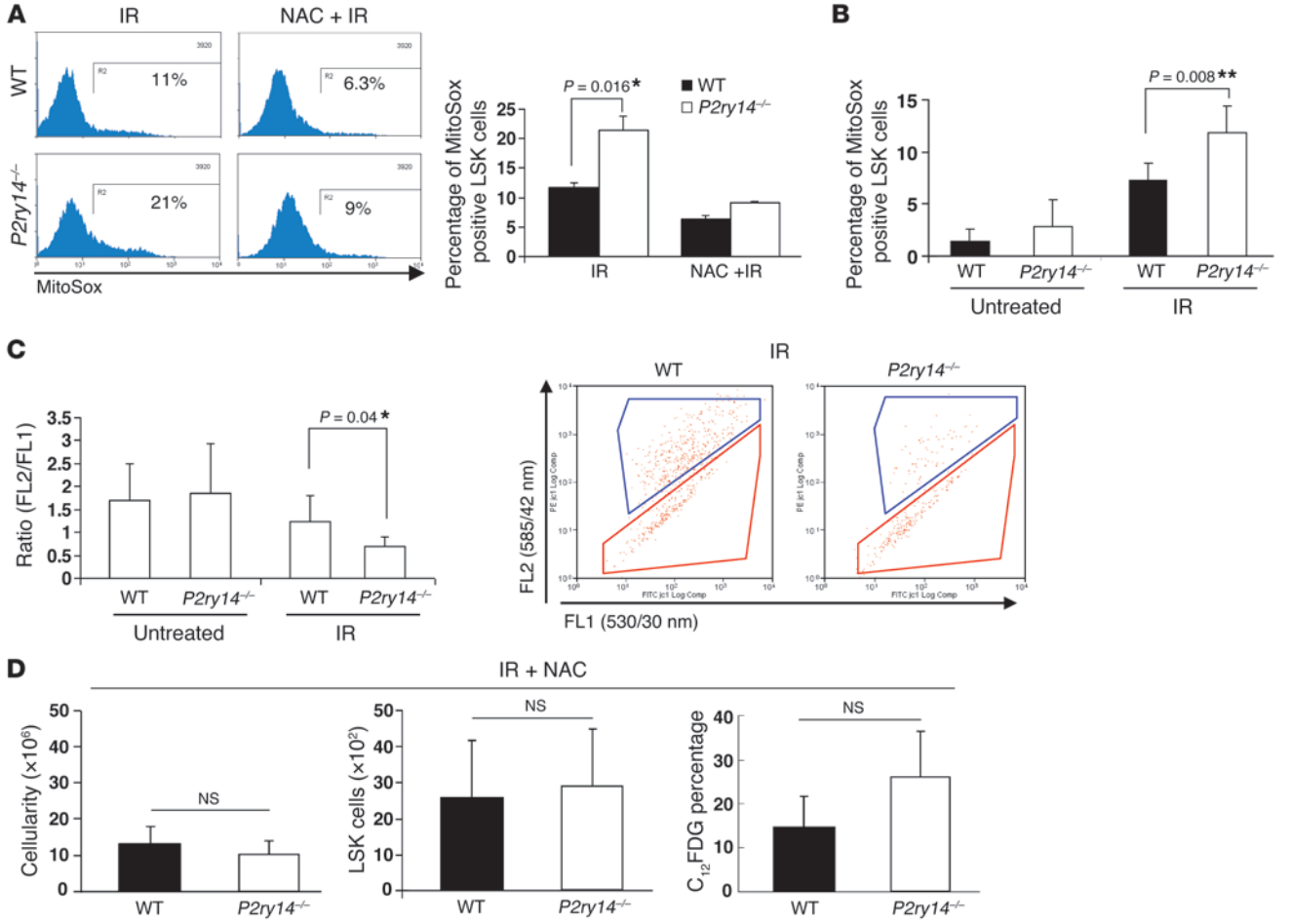

Figure 6

$P2Y_{14}$ is involved in the modulation of cellular redox homeostasis. (**A** and **B**) MitoSOX staining in gated LSK cells. Mitochondrial superoxide was measured within LSK cells in vivo (6 Gy TBI) (**A**) and in vitro (1.6 Gy, in vitro IR) (**B**). NAC was treated as described in the legend to Figure 2. Representative histograms of MitoSOX staining in gated LSK cell (**A**, left). The accompanying graphs show percentage of LSK cells positive for MitoSOX fluorescence in vivo (**A**) and in vitro (**B**). The data are representative of at least 3 independent experiments. The 1-tailed Student's *t* test was used. (**C**) JC-1 staining in gated LSK cells. WT and *P2ry14*$^{-/-}$ BM cells were irradiated as described in **B**. A decrease in the ratio of red (FL2: 585 nm) to green (FL1: 530 nm) indicates mitochondrial depolarization. The data are representative of 3 independent experiments, each with BM cells pooled from at least 2 mice per group. The 1-tailed Student's *t* test was used. (**D**) Mice of the indicated genotypes were exposed to TBI (3 × 5 Gy, 15 days apart). NAC (100 mg/kg) was injected s.c. 4 hours before and 2 hours after TBI and once daily thereafter for 6 days. This procedure was repeated after each TBI. The number of total BM (left) and LSK (middle) cells was counted. Mice (n = 4) were individually analyzed for each group. Right: mice (n = 6/genotype) were exposed to TBI (6 Gy). NAC was administered as described in Figure 2C, and percentage of SA–β-gal$^+$ LSK cells was assessed. *P < 0.05; **P < 0.01.

loss in $P2Y_{14}$ KO embryos following irradiation (IR) can be potentially linked to a differential susceptibility of $P2Y_{14}$ KO embryos to IR-induced premature senescence (23, 24). We therefore determined whether $P2Y_{14}$ KO embryos are more susceptible than their HT or WT littermates to IR-induced senescence by assessing SA–β-gal activity. The level of SA–β-gal was preferentially and markedly elevated in $P2Y_{14}$ KO embryos upon IR (Figure 5B), suggesting that deletion of $P2Y_{14}$ sensitized embryos to IR-induced senescence.

We further assessed senescence induction using mouse embryonic fibroblasts (MEFs) that we also noted abundantly express *P2ry14* mRNA (Supplemental Figure 6). MEFs were subjected to serial passages under standard culture conditions, which supply supraphysiological levels of oxygen (20% O_2). It was reported that this high oxygen level imposes a state of oxidative stress on MEFs, resulting in DNA damage (25). $P2Y_{14}$ KO MEFs exhibited slow proliferation compared with WT MEFs and reached a growth plateau earlier as compared with WT MEFs (Figure 5C). $P2Y_{14}$ deficiency accelerated the rate of senescence in MEFs upon serial passaging, as determined by SA–β-gal staining and typical senescent morphology of large and flat cells (Figure 5D). The senescent phenotype of P2Y14 KO MEF also became apparent following IR treatment when it was compared with that of WT counterparts (Supplemental Figure 7). Taken together, these findings indicate that the senescence-prone phenotype induced by $P2Y_{14}$ deficiency could be observed at both a cellular and whole organism level and is not restricted to hematopoietic cells.

Elucidation of molecular mechanisms underlying the hypersusceptibility of the $P2Y_{14}$ deficient HSPCs to radiation-induced senescence. The forma-

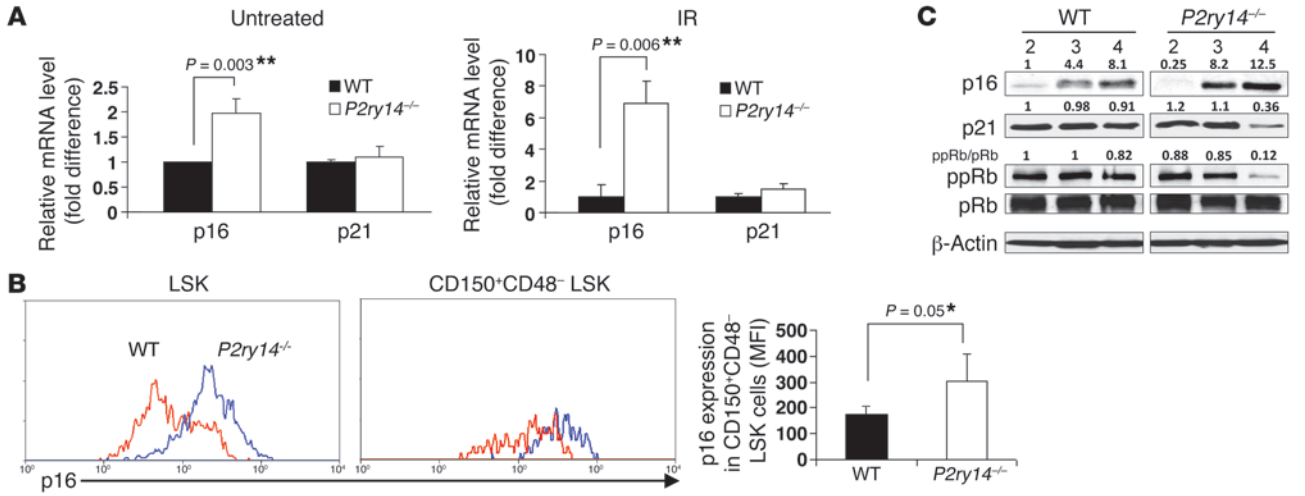

Figure 7

Impact of $P2Y_{14}$ deficiency on senescence-associated molecules. (**A**) WT and *P2ry14*$^{-/-}$ BM cells were transplanted as described. Eight months after transplantation, recipient mice were either left untreated (n = 4, left) or irradiated (n = 4, right) with TBI (6 Gy). LSK cells derived from WT (CD45.1$^+$) or *P2ry14*$^{-/-}$ (CD45.2$^+$) donors in the recipients were sorted and subjected to Q-PCR analysis, respectively. The expression level in WT cells was arbitrarily set to 1. The fold change in expression of each gene was calculated using the ΔΔCt method. The expression was normalized to GAPDH. The 2-tailed Student's t test was used. (**B**) Four weeks after TBI (6 Gy), LSK and CD150$^+$CD48$^-$ LSK cells were gated and analyzed for the expression of p16^{Ink4a} by flow cytometry analysis. Mice were analyzed individually (n > 3 mice/group). Representative flow cytometric analysis of p16^{Ink4a} in gated LSK and CD150$^+$CD48$^-$LSK cells is shown (left). The 2-tailed Student's t-test was used. (**C**) Western blot analysis of WT and *P2ry14*$^{-/-}$ MEF cells: early passage WT or *P2ry14*$^{-/-}$ MEFs were prepared and serially passaged following a 3T3 protocol. Cell lysates were probed with the indicated antibodies. Autoradiographs were analyzed by densitometry. The intensity observed in passage no. 2 WT MEF cells was normalized to the β-actin and arbitrarily set to 1.0. The normalized signal intensities of ppRb and pRb proteins were expressed as a ppRb/pRb ratio. The ratio of ppRb/pRb in passage no. 2 WT MEF cells was arbitrarily set to 1.0. Number denotes passage numbers. *P < 0.05; **P < 0.01.

tion of ROS by radiation is one of the major direct causes of cellular injury. Failure to regulate redox homeostasis accelerates the catastrophic depletion of the stem cell pool. HSCs are especially sensitive to oxidative stress (26), and elevated levels of ROS have been reported to be a major contributing factor toward loss or functional impairment of HSCs in other settings (26–28). Therefore, we investigated whether ROS participates in $P2Y_{14}$ KO HSPC sensitivity to IR. Since mitochondria are the major source of ROS, we assessed mitochondrial ROS levels within LSK cells. Radiation treatment resulted in a significantly higher level of ROS in $P2Y_{14}$ KO LSK cells compared with WT LSK cells both in vivo (Figure 6A, P = 0.016) and in vitro (Figure 6B, P = 0.008). Increased ROS levels negatively affect mitochondrial function, as evident by a drop in mitochondrial membrane potential (Δψm). Dysfunctional mitochondria, in turn, lead to more ROS generation, resulting in a vicious cycle (29). Mitochondrial defects are associated with impaired HSC function (28). $P2Y_{14}$ KO LSK cells were noted to have increased ROS levels in association with low Δψm (Figure 6C), suggesting that ROS and mitochondrial dysfunction combine to compromise HSPC function.

To further test whether IR-induced ROS are indeed responsible for the observed preferential reduction of BM cellularity and LSK cells in $P2Y_{14}$ KO mice, WT and KO mice were treated with a ROS scavenger, N-acetyl-cysteine (NAC). NAC treatment reduced levels of superoxide in LSK cells (Figure 6A) and alleviated IR-induced LSK cell senescence (Figure 6D) and cell death (Figure 2C) in $P2Y_{14}$-deficient LSK cells. This was accompanied with restoration of BM cellularity (Figure 6D) and LSK cell number (Figure 6D). Therefore, ROS is central to functional defects in HSPC seen with $P2Y_{14}$ deficiency.

When cellular senescence is induced, there are typical expression patterns of the cell-cycle regulators (30), including the cyclin-dependent kinase inhibitor p16^{INK4a} (31).

We did not detect differences in expression levels of *p16*^{INK4a} transcripts in freshly prepared $P2Y_{14}$ KO and WT LSK cells (data not shown). When KO cells were transplanted into primary recipients, *p16*^{INK4a} expression began to increase in $P2Y_{14}$ KO LSK cells (a moderate 1.9-fold increase compared with that in WT LSK) (P = 0.003) (Figure 7A). When these primary recipients were subjected to subsequent radiation, $P2Y_{14}$ KO LSK cells displayed a marked increase in *p16*^{INK4a} expression (6- to 8-fold, P = 0.006) (Figure 7A). The observed changes in *p16*^{INK4a} transcripts were paralleled by changes in p16^{Ink4a} protein in LSK and CD150$^+$CD48$^-$ LSK cells, detected by flow cytometric analysis (Figure 7B).

To further determine the nature of premature senescence in $P2Y_{14}$ KO cells at the protein level, MEF cells were analyzed for expression of senescence-associated proteins. With higher passage numbers, elevated levels of p16^{INK4a} protein were observed in $P2Y_{14}$ KO MEFs (Figure 7C). The retinoblastoma protein (pRb) is hypophosphorylated in senescent cells, and its function is necessary for inducing the senescent phenotype (32, 33). It is also reported that the increased expression of p16^{Ink4a} results in the accumulation of hypophosphorylated pRb (34). In line with these findings, hyperphosphorylated forms of RB (ppRb) became significantly lower in $P2Y_{14}$ KO MEFs at passage 4 (see the ratio of ppRb to pRb in Figure 7C).

Hyperradiosensitivity of $P2Y_{14}$ KO HSPCs may relate to their differential DNA repair capacity. However, similar levels of DNA damage (at 30 minutes after IR) and repair (at 6 hours after IR), as mea-

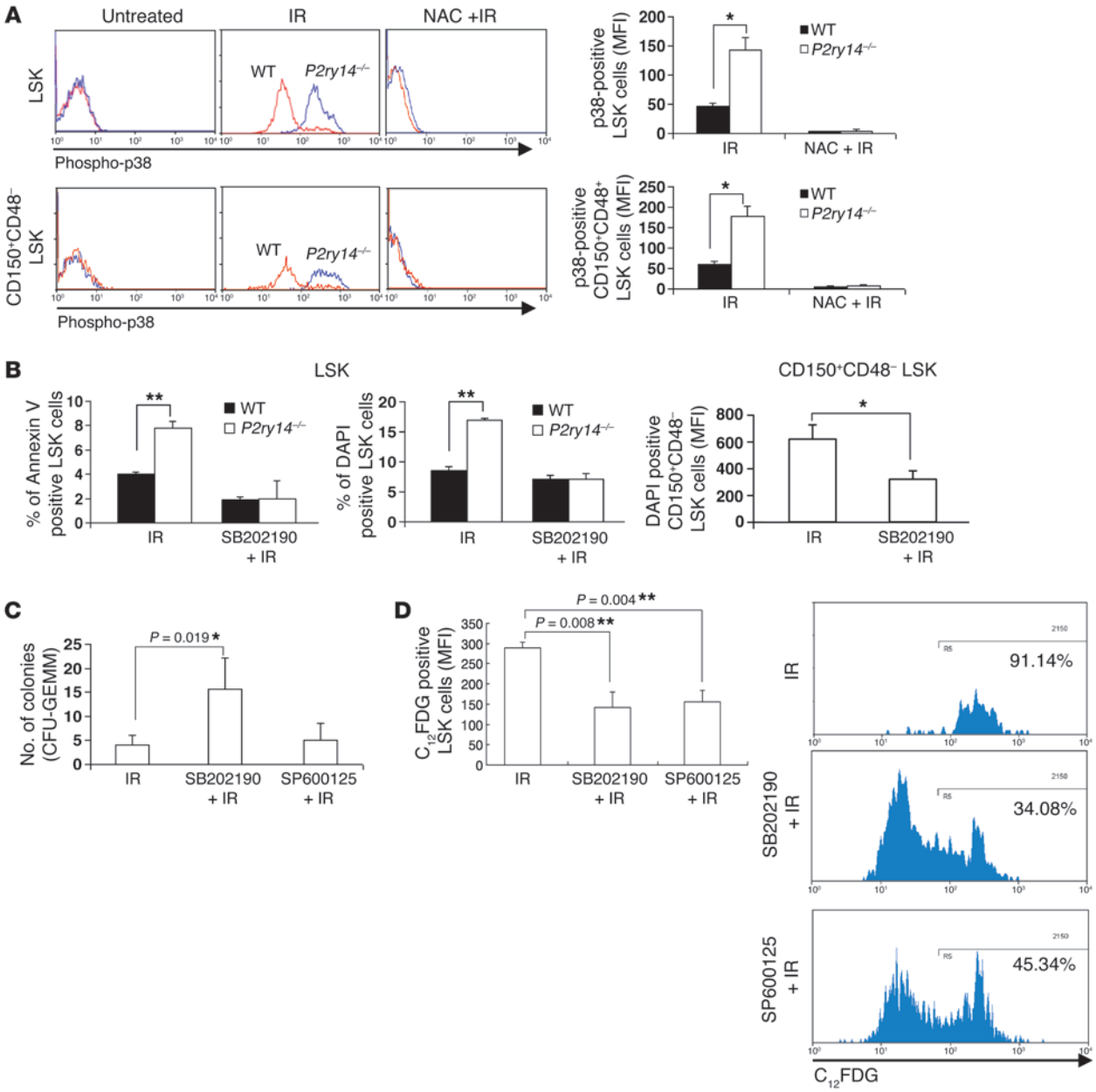

Figure 8

Analysis of molecular pathways underlying the increased susceptibility of $P2Y_{14}$-deficient HSPCs to radiation. (**A**) WT (red lines) and *P2ry14*$^{-/-}$ (blue lines) mice were exposed to TBI (6 Gy). Mice (n > 4 mice/genotype) were sacrificed immediately after IR and their LSK (upper) and $CD150^+CD48^-$ LSK (lower) cells were analyzed for phosphorylated p38 MAPK by flow cytometry. NAC was treated as described. The accompanying graphs (right) show the MFI of phospho–p38 MAPK in LSK (upper) and $CD150^+CD48^-$ LSK (lower) cells. (**B** and **C**) Irradiated WT and KO mice (6 Gy) were sacrificed 8 hours after IR and their LSK and $CD150^+CD48^-$ LSK cells were analyzed for cell death. Representative dot plots and histograms are shown in Supplemental Figure 10. p38 MAPK inhibitor (SB202190) and JNK inhibitor (SP600125) were administered 30 minutes before and immediately after TBI. (**C**) Clonogenic capacity of the treated cells was analyzed by CFU assay. (**D**) $P2Y_{14}$ KO mice were exposed to TBI (6 Gy). SB202190 and SP600125 were administered as described above. Mice were sacrificed 30 minutes after IR, and their BM cells were transplanted into recipient mice (n > 5/each group). LSK cells were analyzed at 4 to 5 weeks after transplantation for C_{12}FDG expression. P values in Figure 8 were determined using 2-tailed Student's t test. *P < 0.05; **P < 0.01.

sured through the γ-H2AX assay, were detected in $P2Y_{14}$ KO HSPCs in comparison with WT counterparts (Supplemental Figure 8), arguing against an altered response or ability to repair DNA double-strand breaks. There were no cell-cycle differences detected between WT and KO LSKs either before or after IR (Supplemental Figure 9).

p38 MAPK has been shown to act downstream of ROS, and its activation in HSC can lead to a defect in HSCs (26, 27). It is also a known mediator of the cytokine release phenomena associated with senescence (35). We thus determined whether $P2Y_{14}$ KO HSPCs display differential activation of p38 MAPK under

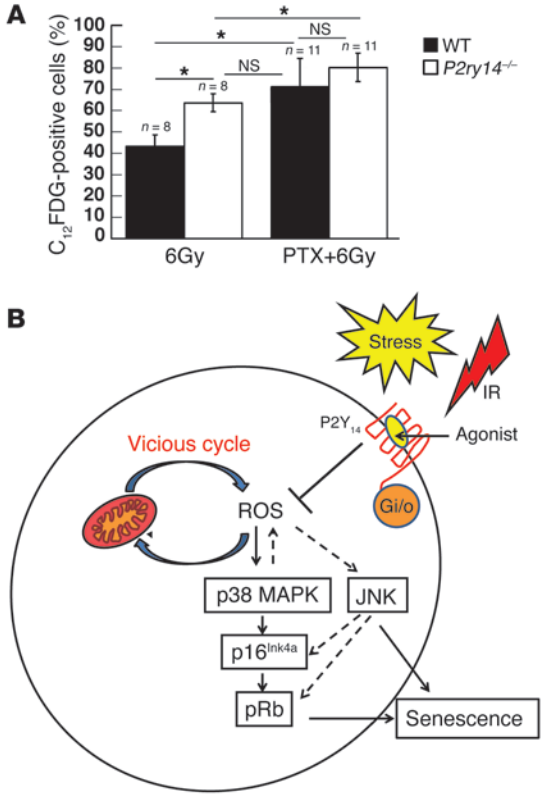

Figure 9

$P2Y_{14}$ signals through Gi/o to modulate IR-induced HSPC senescense. (**A**) Thirty minutes after PTX injection, the mice were subjected to 6 Gy TBI. The BM cells (CD45.2) were immediately harvested and transplanted into recipient mice (CD45.1.2). Recipients were sacrificed 9 to 14 days after transplantation. Donor-derived ($CD45.2^+$) WT and KO LSK cells were analyzed for C_{12}FDG expression. (**B**) A simplified schema of the proposed model. The $P2Y_{14}$ receptor couples to Gi/o proteins and inhibits stress-induced (e.g., IR) ROS formation restraining SIPS. In contrast, the high levels of ROS are accumulated in $P2Y_{14}$-deficient cells by stress and cause mitochondrial dysfunction. This in turn triggers further accumulation of ROS, leading to a vicious cycle. Increased ROS levels mediate the hyperactivation of p38 MAPK, which may in turn mediate the p16/pRb-dependent senescence pathway. JNK activation may potentially be involved in SIPS. Arrows denote activation, and the blunted lines indicate inhibition. Dotted lines denote possible pathways that have not yet been demonstrated. *$P < 0.05$.

radiation stress. Since ROS generation occurs within seconds of radiation exposure and persists for 2 to 5 minutes after IR (36), the activation of p38 MAPK was analyzed at an early time point immediately after TBI. While there was no detectable difference in p38 MAPK activity between WT and KO HSPCs under homeostatic conditions, p38 MAPK activity was notably higher in $P2Y_{14}$-deficient LSK and $CD150^+CD48^-$ LSK cells following radiation (Figure 8A). Of note, p38 MAPK activation was transient, as its level returned to near basal control levels about 5 hours after TBI (data not shown). To investigate whether this aberrant activation of the p38 MAPK in $P2Y_{14}$-deficient HSPCs accounts for their increased susceptibility to IR, a specific p38 MAPK inhibitor was administered to animals. p38 MAPK inhibitor treatment not only reduced the susceptibility of $P2Y_{14}$-deficient LSK and $CD150^+CD48^-$ LSK cells to IR-induced cell death (Figure 8B and Supplemental Figure 10), but also restored their clonogenic capacity (Figure 8C). Furthermore, p38 MAPK inhibition significantly ameliorated the susceptibility of $P2Y_{14}$ KO HSPCs to IR-induced senescence (Figure 8D). Of note, NAC treatment almost completely abolished the p38 MAPK activation in HSPCs (Figure 8A). Both p38 MAPK and c-JNK are known to be activated by IR and share many common signaling components (37). However, p38 MAPK and JNK can mediate distinct stress responses depending on the nature and duration of the stress and the cellular context (38). The inhibition of JNK with its inhibitor, SP600125, did not exert any measurable effect on clonogenic capacity (Figure 8C), but was able to reduce IR-induced LSK cell senescence (Figure 8D). These data are consistent with $P2Y_{14}$ limiting radiation-induced activation of p38 MAPK and JNK, perhaps by reducing ROS.

While the signaling pathways triggered by the $P2Y_{14}$ receptor are still poorly documented, it is reported that $P2Y_{14}$ receptor exerts its effects primarily via the Gi/o family of the heterotrimeric G protein family (39, 40). To determine whether the increased sensitivity of $P2Y_{14}$ KO HSPCs to IR is mediated via the $P2Y_{14}$ receptor acting through Gi/o, $P2Y_{14}$ KO and WT mice were injected with pertussis toxin (PTX) and then exposed to 6 Gy TBI. BM cells (CD45.2) were harvested and subsequently transplanted into recipient animals (CD45.1.2). We then examined the effects of PTX treatment on IR-induced HSPC senescence. Since PTX specifically inactivates Gi/o-mediated signaling pathways (39), one would expect that interruption of Gi/o signaling in WT cells by PTX would recapitulate the phenotype of KO HSPCs in response to IR-induced senescence, if the observed difference is mediated via $P2Y_{14}$ receptor. As shown in Figure 9A, upon PTX treatment, WT cells demonstrated senescence induction similar to that of KO cells. Also, the difference between WT and KO LSK cells was abrogated, with PTX supporting the notion that $P2Y_{14}$ signals through Gi/o to modulate IR-induced LSK cell senescence.

Taken together, our data support the hypothesis that the Gi/o-coupled $P2Y_{14}$ signaling axis modulates stress-induced HSPC senescence, at least in part, through a mechanism involving ROS, p38 MAPK/JNK, and p16/Rb (Figure 9B).

Discussion

Stem cells possess the capacity to replenish damaged or dysfunctional cells throughout life. However, stem cells are themselves vulnerable to stress-mediated cellular injury, and a progressive diminution of stem cells in response to stress leads to loss of tissue homeostasis. Therefore, preserving the integrity of HSC function is closely associated with morbidity and mortality in patients receiving radiation and chemotherapy. Despite these significant clinical implications, the molecular machinery of how stem cells cope and adapt to the various types of stress is poorly defined.

In this study, we demonstrate that a purinergic receptor, $P2Y_{14}$, plays an indispensable role in counteracting the deleterious effects of multiple types of cell stress in HSPCs.

Under physiological conditions, $P2Y_{14}$ appears to not be essential for normal embryonic development nor for the maintenance of tissue homeostasis in the adult organism. However, the embryo is exceptionally sensitive to radiation-induced damage, and under the stress conditions of TBI, $P2Y_{14}$ KO embryos were more prone to undergoing IR-induced senescence than WT embryos.

In the adult, hematopoietic cells are among the most sensitive to radiation injury. $P2Y_{14}$ KO mice were more sensitive to radiation,

showing a more severe reduction in the number of BM cells than that observed in WT mice. This was accompanied by a more profound reduction of LSK cells in $P2Y_{14}$ KO mice, suggesting that loss of $P2Y_{14}$ confers increased susceptibility to radiation in HSPC populations. $P2Y_{14}$ KO mice were also hypersensitive to other hematological stress. The response of $P2Y_{14}$ KO mice to 5-FU treatment documented a higher susceptibility of $P2Y_{14}$ KO HSPCs to repetitive myelotoxic stress. Furthermore, $P2Y_{14}$ KO BM cells were outcompeted by WT BM cells in secondary recipient animals. Taken together, these results suggest that $P2Y_{14}$ KO HSPCs are functionally compromised in their ability to cope with hematological stress.

A sublethal dose of TBI induces HSC senescence (13), and $P2Y_{14}$ KO HSPCs showed typical phenotypic and molecular changes associated with cellular senescence upon IR, suggesting that the differential response of $P2Y_{14}$ KO cells to IR may be due to their increased sensitivity to IR-induced senescence. However, senescent cells eventually undergo apoptosis, so that the accumulation of senescent cells can also lead to increased apoptosis in $P2Y_{14}$ KO mice. While $P2Y_{14}$ is expressed in a relatively small fraction of LSK and $CD150^+CD48^-$ LSK cells (Figure 1B), the difference in IR-induced senescence phenotype was detectable in a larger fraction of HSPCs. One potential explanation for this might be due to the increased expression of $P2Y_{14}$ in a subset of irradiated HSPCs. Indeed, as demonstrated by previous reports (17, 21) and our results here (Supplemental Figure 4), IR and other stress cause the increase of $P2Y_{14}$ expression in stressed cells. It may also be possible that our antibody-based criteria for defining $P2Y_{14}$-expressing cells in Figure 1B underestimate the fraction of cells with a functionally meaningful level of the protein.

Radiation induces cellular injury mainly through the generation of ROS, which is a common mediator of cellular senescence (41). HSCs are much more sensitive to oxidative stress than the progenitors (26), and excessive levels of ROS are especially detrimental to HSCs. The functional defects of HSCs observed in *ATM*-, *Bmi-1*–, and *Foxo*-deficient mice are all attributed to ROS-induced oxidative damage (26, 27, 42), underscoring the crucial role of ROS in stem cell injury. A higher level of mitochondrial ROS was detected in $P2Y_{14}$ KO LSK cells than in WT counterparts following IR. Consequently, it caused a significant loss of $\Delta\psi m$ in $P2Y_{14}$ KO LSK cells. Meanwhile, the antioxidant NAC markedly attenuated IR-induced HSPC depletion and senescence in $P2Y_{14}$ KO mice, suggesting that the increased sensitivity of $P2Y_{14}$ KO cells to IR stress is likely attributable, at least in part, to dysregulation of ROS in $P2Y_{14}$ KO cells following TBI.

There was a differential activation of p38 MAPK between $P2Y_{14}$ KO and WT LSK cells following IR. Since p38 MAPK activation in HSC can lead to a defect in HSCs (26, 27), ROS-induced hyperactivation of p38 MAPK in $P2Y_{14}$-deficient HSPCs is a potential mechanism underlying the increased susceptibility to IR stress. While we were unable to detect JNK activation in HSPC cells due to the lack of specific antibody that works for flow cytometry analysis, JNK inhibition was found to significantly reduce IR-induced HSPC senescence, suggesting a role of JNK as another potential $P2Y_{14}$ downstream modulator in IR-induced HSPC senescence. While p38 MAPK is known to play significant roles in regulating stress-induced HSPC senescence (43), the role of the JNK in SIPS is controversial (44, 45). The mechanism that enables JNK to mediate SIPS in HSPC is beyond the scope of this study. The net effects of JNK on SIPS may vary depend on the individual cellular context, intensity, and duration of JNK.

Purinergic receptors serve as sensitive sensors for cell/tissue damage and have been proposed to function as early alarm signals (9, 46, 47). Interestingly, while most of the purinergic receptors in KO mice display no aberrant phenotype under homeostatic conditions (48), the phenotypic consequences of their deficiencies become evident when KO mice are subjected to ischemia (49), infection (50), or bleeding (51, 52), suggesting the pivotal roles of purinergic receptor in a variety of pathophysiological conditions.

UDP-glucose (UDP-Glc) has been proposed as a ligand for the $P2Y_{14}$ receptor (53). Since extracellular UDP-Glc is at high levels following mechanical stress of cells (54) or with cultured tumor cells (55), it is possible that high levels of extracellular UDP-Glc may accompany local tissue stress, triggering $P2Y_{14}$ downstream cellular responses. Since cellular response to external UDP-Glc could vary depending on dose and time of administration, more detailed pharmacokinetic and metabolic studies of UDP-Glc would be required to determine whether UDP-Glc is a functionally relevant endogenous ligand in the context of IR-induced senescence. It should also be noted that controversy exists as to whether UDP-Glc is a functionally relevant ligand for the $P2Y_{14}$ receptor (56, 57) raising the possibility of an as-yet-unknown $P2Y_{14}$ ligand or ligands. Furthermore, a recent study showed that UDP-Glc can function through $P2Y_{14}$ receptor–dependent and –independent mechanisms in the gastrointestinal (GI) tract (15). Multiple ligands are common to most of G protein coupled receptors (GPCRs), and the existence of physiologically distinct ligands for $P2Y_{14}$ remains a possibility.

While receptor activation inhibiting apoptosis is a well-known phenomenon, the concept of a receptor whose activation inhibits senescence has little precedent in mammals, to our knowledge, and is of interest.

Based on the ability of stem cells to repair or rejuvenate age-related tissue damage, it is conceivable that stem cell aging contributes to tissue aging. However, the issue of whether or not stem cell aging correlates with organismal aging is still the subject of debate, since the pool size and regenerative capacity of tissue-specific stem cells do not necessarily predict the life span of an organism (58). The present study shows how $P2Y_{14}$ deficiency affected radiation-induced senescence in a subset of HSPC cells. Therefore, without further data, it is premature to predict whether $P2Y_{14}$ has an impact on tissue or organismal aging.

Whether receptor alteration of cellular stress tolerance can have other physiologic effects is yet to be explored in our mammalian model. However, it is of interest that the invertebrate gene *Methuselah* is also a GPCR that modulates cellular response to varying types of stress and is a known regulator of life span in *Drosophila melanogaster* (59). Whether $P2Y_{14}$ may serve as a mammalian parallel of a receptor signaling in response to extracellular conditions, thereby modulating the impact of stress on organismal function and aging, is an intriguing issue for future study.

Methods

Animals and treatment. $P2Y_{14}$ mice (15) were kindly provided under material transfer agreement (MTA) by GlaxoSmithKlein (Platform Technology and Science). Briefly, the mouse *P2ry14* gene (892 bp of coding sequence) was deleted by replacement with the IRES-lacZ-polyA-neo cassette, resulting in the removal of the last 6 predicted TM domains out of the 7-transmembrane domain of $P2Y_{14}$ protein. Homozygous KO mice were obtained by mating HT. Unless otherwise stated, all experiments were performed with littermates as control. The genotyping was performed by PCR analysis as

previously described (15). NAC (100 mg/kg) was injected s.c. p38 MAPK inhibitor (SB202190, 2 mg/kg) and JNK inhibitor (SP-600125, 10 mg/kg) were administered i.p. 30 minutes before and immediately after TBI. $P2Y_{14}$ WT and KO mice were injected i.v. with a single dose of PTX (0.8–1 mg/mouse) 30 minutes before TBI (6 Gy). BM cells were isolated immediately after TBI and transplanted into recipient animals (CD45.1.2).

CFU assays. BM cells were seeded at a concentration of 1.5×10^4/35 mm dish for CFU-GEMM assay (Methocult 3434, Stem Cell Tech.). All assays were performed in triplicate. The colonies were counted on day 12.

Competitive long-term repopulating cell assay. Competitive repopulation assay was performed using CD45.1.2 mice as recipients, which were generated by mating SJL CD45.1 female with B6(cg)-Tyrc-2j/J CD45.2 male mice. BM cells from $P2Y_{14}$ mice (B6, CD45.2) were mixed with congenic competitor cells (B6, CD45.1) and then transplanted into lethally irradiated (10–11 Gy) recipient mice (CD45.1.2). *P2ry14*$^{-/-}$ BM contains a higher frequency of HSPCs than WT BM (Supplemental Figure 3). When *P2ry14*$^{-/-}$ BM cells were mixed at a 1:1.2–1.3 ratio with congenic WT BM cells, equal contributions from the WT versus *P2ry14*$^{-/-}$ cells are seen in PB of recipient mice over a 1-year post-transplant period. PB and/or BM cells were collected from recipient mice at various stages of posttransplant periods and treatments, and the ratio of CD45.1/CD45.2 was assessed by flow cytometry (Beckman Coulter).

Antibodies and flow cytometry. The cells were stained with lineage antibody cocktails and c-Kit and Sca-1 antibodies. The following lineage antibodies were purchased from e-Bioscience: PE-Cy7–conjugated anti-CD3 (CT-CD3), anti-CD4 (CT-CD4), anti-CD8 (CT-CD8a), anti-CD45R (RA3-6B2), anti-CD11b (M1/70.15), anti–Gr-1 (RB6-8C5), and anti–TER-119 (TER-119). Sca-1 and c-Kit antibodies were from BD Biosciences — Pharmingen. FITC or PE–Texas red–conjugated anti-CD34 (RAM34) antibodies were from e-Bioscience. Percp-cy5.5–conjugated anti-CD150 (TC15-12F12.2) and Pacific blue–conjugated anti-CD48 (HM48-1) antibodies were from Biolegend. FITC-conjugated anti-$p16^{INK4a}$ was purchased from Santa Cruz Biotechnology Inc. Pacific blue–conjugated anti–p38 MAPK was from Cell Signaling. LSK cells were sorted by MoFlo (DakoCytomation). $P2Y_{14}$ antibody (Alomone Labs) was biotinylated with EZ-Link Micro-PEO_4-Biotinylation Kit (Thermo Scientific). PE-conjugated streptavidin antibody (eBioscience) was used as a secondary antibody.

Q–RT-PCR. Cells were stained with fluorescently labeled antibodies, as indicated. and directly sorted into PCR tubes containing lysis buffer. RNA was isolated using RNeasy Micro kit (QIAGEN) from sorted cells. Reverse transcription of RNA was performed using QuantiTech Reverse Transcription Kit (QIAGEN). All primers for Q-PCR were purchased from Applied Biosystems.

Immunoblotting. MEFs were collected at each passage. Cell lysates were subjected to SDS-PAGE analysis. Primary antibodies for $p16^{INK4a}$, $p21^{Cip1}$, pRb, and ppRb were purchased from Santa Cruz Biotechnology Inc.

ROS, apoptosis, JC-1 analysis. Five to eight hours after IR treatment, BM cells were stained with lineage antibody cocktails and c-Kit and Sca-1 antibodies. For the measurement of mitochondrial ROS, MitoSOX Red (Molecular Probes) was applied to LSK cells (5 μM final concentration) that were stained with APC-conjugated anti–c-Kit, FITC-conjugated anti–Sca-1, and PE/Cy7-conjugated anti-lineage markers. For apoptosis analysis, the cells were stained using the Annexin V Apoptosis Detection Kit I (BD Biosciences — Pharmingen). For the study of $\Delta\psi m$, MitoProbe JC-1 Assay Kit (Molecular Probes) was used. Briefly, JC-1 was applied to LSK cells (2 μM final concentration) that were stained with APC-conjugated anti–c-Kit, PerCp/Cy5.5-conjugated anti–Sca-1, and PE/Cy7-conjugated anti-lineage markers. JC-1 ratio was evaluated by FL2/FL1 (red/green) using flow cytometry.

SA–β-gal staining. MEF cells were incubated with SA–β-gal solution (1 mg/ml X-gal, 5 mM potassium ferricyanide, 5 mM potassium ferrocyanide, 150 mM NaCl, and 2 mM $MgCl_2$ in PBS, pH 6.0) overnight at 37°C and then observed under a light microscope. For embryo staining, embryos (E18.5) were fixed in 4% paraformaldehyde for 30 minutes on ice and stained as described above. Donor-derived ($CD45.2^+$) LSK and $CD150^+CD48^-$ LSK cells were analyzed for SA–β-gal activity using a fluorogenic β-gal substrate, C_{12}FDG (Molecular Probes), as previously described (60, 61). Briefly, cells were stained for LSK and $CD150^+CD48^-$ LSK cells as indicated above, followed by C_{12}FDG staining at a final concentration of 33 μM.

Cell-cycle analysis. BM cells were stained for LSK cells and fixed with Cytofix/Cytoperm buffer (BD Biosciences — Pharmingen). After washing once with Perm/Wash buffer (BD Biosciences — Pharmingen), cells were permeabilized with Cytoperm Plus buffer (BD Biosciences — Pharmingen). Cells were then incubated with Ki-67 antibody (BD Biosciences — Pharmingen) for 30 minutes at room temperature, which was followed by DAPI (Invitrogen) staining.

Serial transplantation. All recipient animals were conditioned as described above. At 2 months after transplantation, BM cells from primary recipients were pooled and transplanted into secondary recipient animals.

Statistics. Data are expressed as mean ± SD. and *P* values were determined by 1-tailed or 2-tailed Student's *t* test as indicated in the figure legends. $P < 0.05$ was considered significant.

Study approval. All studies were approved by GlaxoSmithKlein, the Harvard Stem Cell Institute, and the University of Pittsburgh's IACUC and were in accordance with GlaxoSmithKlein, Harvard University, and the University of Pittsburgh's policies on the care, welfare, and treatment of laboratory animals.

Acknowledgments

The authors are grateful to Yong Wang and Daehong Zhou for providing detailed experimental protocols for the flow cytometry detection of p16. We thank Alastair Morrison and GlaxoSmithKlein for *P2ry14* mice. This work was supported in part by the Department of Defense (W81XWH-09-1-0364 to B.C. Lee); and by the National Basic Research Program (2011CB964800) and the National Natural Science Foundation of China (NSFC 81090410) (to T. Cheng). B.C. Lee is a recipient of the Junior Investigator Award from the Department of Medicine, University of Pittsburgh School of Medicine. This project used the University of Pittsburgh Cancer Institute flow cytometry and animal facility, which was supported in part by an award from the NIH (P30CA047904).

Received for publication February 21, 2014, and accepted in revised form April 29, 2014.

Address correspondence to: Byeong Chel Lee, University of Pittsburgh Cancer Institute, Hillman Cancer Center, 5117 Centre Avenue, Pittsburgh, Pennsylvania 15213, USA. Phone: 412.623.2285; Fax: 412.623.7828; E-mail: leeb4@upmc.edu. Or to: David Scadden, Massachusetts General Hospital, Center for Regenerative Medicine, 185 Cambridge Street, CPZN-4265A, Boston, Massachusetts 02114, USA. Phone: 617.726.5615; Fax: 617.724.2662; E-mail: david_scadden@harvard.edu.

1. Volonte C, Amadio S, D'Ambrosi N, Colpi M, Burnstock G. P2 receptor web: complexity and fine-tuning. *Pharmacol Ther*. 2006;112(1):264–280.
2. Abbracchio MP, Burnstock G. Purinergic signalling: pathophysiological roles. *Jpn J Pharmacol*. 1998;78(2):113–145.
3. Elliott MR, et al. Nucleotides released by apoptotic cells act as a find-me signal to promote phagocytic clearance. *Nature*. 2009;461(7261):282–286.
4. White N, Burnstock G. P2 receptors and cancer. *Trends Pharmacol Sci*. 2006;27(4):211–217.
5. Webb TE, Simon J, Bateson AN, Barnard EA. Transient expression of the recombinant chick brain P2y1 purinoceptor and localization of the corresponding mRNA. *Cell Mol Biol (Noisy-le-grand)*. 1994;

40(3):437–442.
6. Devader C, Drew CM, Geach TJ, Tabler J, Townsend-Nicholson A, Dale L. A novel nucleotide receptor in Xenopus activates the cAMP second messenger pathway. *FEBS Lett*. 2007;581(27):5332–5336.
7. Erb L, Liao Z, Seye CI, Weisman GA. P2 receptors: intracellular signaling. *Pflugers Arch*. 2006; 452(5):552–562.
8. Brunschweiger A, Muller CE. P2 receptors activated by uracil nucleotides — an update. *Curr Med Chem*. 2006;13(3):289–312.
9. Di Virgilio F, et al. Nucleotide receptors: an emerging family of regulatory molecules in blood cells. *Blood*. 2001;97(3):587–600.
10. Sak K, Boeynaems JM, Everaus H. Involvement of P2Y receptors in the differentiation of haematopoietic cells. *J Leukoc Biol*. 2003;73(4):442–447.
11. Di Leonardo A, Linke SP, Clarkin K, Wahl GM. DNA damage triggers a prolonged p53-dependent G1 arrest and long-term induction of Cip1 in normal human fibroblasts. *Genes Dev*. 1994;8(21):2540–2551.
12. Suzuki K, Mori I, Nakayama Y, Miyakoda M, Kodama S, Watanabe M. Radiation-induced senescence-like growth arrest requires TP53 function but not telomere shortening. Radiat Res. 2001; 155(1 pt 2):248–253.
13. Wang Y, Schulte BA, LaRue AC, Ogawa M, Zhou D. Total body irradiation selectively induces murine hematopoietic stem cell senescence. *Blood*. 2006; 107(1):358–366.
14. Lee BC, et al. P2Y-like receptor, GPR105 (P2Y14), identifies and mediates chemotaxis of bone-marrow hematopoietic stem cells. *Genes Dev*. 2003; 17(13):1592–1604.
15. Bassil AK, et al. UDP-glucose modulates gastric function through P2Y14 receptor-dependent and -independent mechanisms. *Am J Physiol Gastrointest Liver Physiol*. 2009;296(4):G923–G930.
16. Kook S, Cho J, Lee SB, Lee BC. The nucleotide sugar UDP-glucose mobilizes long-term repopulating primitive hematopoietic cells. *J Clin Invest*. 2013;123(8):3420–3435.
17. Charlton ME, Williams AS, Fogliano M, Sweetnam PM, Duman RS. The isolation and characterization of a novel G protein-coupled receptor regulated by immunologic challenge. *Brain Res*. 1997; 764(1–2):141–148.
18. Zhuang W, Qin Z, Liang Z. The role of autophagy in sensitizing malignant glioma cells to radiation therapy. *Acta Biochim Biophys Sin (Shanghai)*. 2009;41(5):341–351.
19. Allsopp RC, Morin GB, Horner JW, DePinho R, Harley CB, Weissman IL. Effect of TERT over-expression on the long-term transplantation capacity of hematopoietic stem cells. *Nat Med*. 2003;9(4):369–371.
20. Cheung KK, Ryten M, Burnstock G. Abundant and dynamic expression of G protein-coupled P2Y receptors in mammalian development. *Dev Dyn*. 2003;228(2):254–266.
21. Kook SH, et al. The purinergic P2Y14 receptor axis is a molecular determinant for organism survival under in utero radiation toxicity. *Cell Death Dis*. 2013;4:e703.
22. Wang B, et al. Adaptive response in embryogenesis: I. Dose and timing of radiation for reduction of prenatal death and congenital malformation during the late period of organogenesis. *Radiat Res*. 1998; 150(1):120–122.
23. MacIntosh C, Morley JE, Chapman IM. The anorexia of aging. *Nutrition*. 2000;16(10):983–995.
24. Luyckx VA, Compston CA, Simmen T, Mueller TF. Accelerated senescence in kidneys of low-birth-weight rats after catch-up growth. *Am J Physiol Renal Physiol*. 2009;297(6):F1697–F1705.
25. Parrinello S, Samper E, Krtolica A, Goldstein J, Melov S, Campisi J. Oxygen sensitivity severely limits the replicative lifespan of murine fibroblasts. *Nat Cell Biol*. 2003;5(8):741–747.
26. Tothova Z, et al. FoxOs are critical mediators of hematopoietic stem cell resistance to physiologic oxidative stress. *Cell*. 2007;128(2):325–339.
27. Ito K, et al. Regulation of oxidative stress by ATM is required for self-renewal of haematopoietic stem cells. *Nature*. 2004;431(7011):997–1002.
28. Liu J, et al. Bmi1 regulates mitochondrial function and the DNA damage response pathway. *Nature*. 2009;459(7245):387–392.
29. Lin MT, Beal MF. Mitochondrial dysfunction and oxidative stress in neurodegenerative diseases. *Nature*. 2006;443(7113):787–795.
30. Wei W, Herbig U, Wei S, Dutriaux A, Sedivy JM. Loss of retinoblastoma but not p16 function allows bypass of replicative senescence in human fibroblasts. *EMBO Rep*. 2003;4(11):1061–1066.
31. Alcorta DA, Xiong Y, Phelps D, Hannon G, Beach D, Barrett JC. Involvement of the cyclin-dependent kinase inhibitor p16 (INK4a) in replicative senescence of normal human fibroblasts. *Proc Natl Acad Sci U S A*. 1996;93(24):13742–13747.
32. Campisi J. Cellular senescence as a tumor-suppressor mechanism. *Trends Cell Biol*. 2001;11(11):S27–S31.
33. Lowe SW, Sherr CJ. Tumor suppression by Ink4a-Arf: progress and puzzles. *Curr Opin Genet Dev*. 2003;13(1):77–83.
34. Lazzerini Denchi E, Attwooll C, Pasini D, Helin K. Deregulated E2F activity induces hyperplasia and senescence-like features in the mouse pituitary gland. *Mol Cell Biol*. 2005;25(7):2660–2672.
35. Freund A, Patil CK, Campisi J. p38MAPK is a novel DNA damage response-independent regulator of the senescence-associated secretory phenotype. *EMBO J*. 2011;30(8):1536–1548.
36. Leach JK, Black SM, Schmidt-Ullrich RK, Mikkelsen RB. Activation of constitutive nitric-oxide synthase activity is an early signaling event induced by ionizing radiation. *J Biol Chem*. 2002;277(18):15400–15406.
37. Munshi A, Ramesh R. Mitogen-Activated Protein Kinases and Their Role in Radiation Response. *Genes Cancer*. 2013;4(9–10):401–408.
38. Murai H, et al. Differential response of heat-shock-induced p38 MAPK and JNK activity in PC12 mutant and PC12 parental cells for differentiation and apoptosis. *Acta Med Okayama*. 2010;64(1):55–62.
39. Carter RL, et al. Quantification of Gi-mediated inhibition of adenylyl cyclase activity reveals that UDP is a potent agonist of the human P2Y14 receptor. *Mol Pharmacol*. 2009;76(6):1341–1348.
40. Burnstock G. Purine and pyrimidine receptors. *Cell Mol Life Sci*. 2007;64(12):1471–1483.
41. Lu T, Finkel T. Free radicals and senescence. *Exp Cell Res*. 2008;314(9):1918–1922.
42. Miyamoto K, et al. Foxo3a is essential for maintenance of the hematopoietic stem cell pool. *Cell Stem Cell*. 2007;1(1):101–112.
43. Wang Y, Liu L, Zhou D. Inhibition of p38 MAPK attenuates ionizing radiation-induced hematopoietic cell senescence and residual bone marrow injury. *Radiat Res*. 2011;176(6):743–752.
44. Debacq-Chainiaux F, Boilan E, Dedessus Le Moutier J, Weemaels G, Toussaint O. p38(MAPK) in the senescence of human and murine fibroblasts. *Adv Exp Med Biol*. 2010;694:126–137.
45. Zubova SG, et al. [Sodium butyrate do not induce the program of premature senescence in transformants with JNK1,2 knockout]. *Tsitologiia*. 2008; 50(11):964–971.
46. Tsuda M, et al. P2X4 receptors induced in spinal microglia gate tactile allodynia after nerve injury. *Nature*. 2003;424(6950):778–783.
47. He L, Chen J, Dinger B, Stensaas L, Fidone S. Effect of chronic hypoxia on purinergic synaptic transmission in rat carotid body. *J Appl Physiol*. 2006; 100(1):157–162.
48. Burnstock G. Purinergic signalling and disorders of the central nervous system. *Nat Rev Drug Discov*. 2008;7(7):575–590.
49. Melani A, et al. P2X7 receptor modulation on microglial cells and reduction of brain infarct caused by middle cerebral artery occlusion in rat. *J Cereb Blood Flow Metab*. 2006;26(7):974–982.
50. Geary C, Akinbi H, Korfhagen T, Fabre JE, Boucher R, Rice W. Increased susceptibility of purinergic receptor-deficient mice to lung infection with Pseudomonas aeruginosa. *Am J Physiol Lung Cell Mol Physiol*. 2005;289(5):L890–L895.
51. Fabre JE, et al. Decreased platelet aggregation, increased bleeding time and resistance to thromboembolism in P2Y1-deficient mice. *Nat Med*. 1999; 5(10):1199–1202.
52. Andre P, et al. P2Y12 regulates platelet adhesion/activation, thrombus growth, and thrombus stability in injured arteries. *J Clin Invest*. 2003;112(3):398–406.
53. Fricks IP, Carter RL, Lazarowski ER, Harden TK. Gi-dependent cell signaling responses of the human P2Y14 receptor in model cell systems. *J Pharmacol Exp Ther*. 2009;330(1):162–168.
54. Lazarowski ER, Shea DA, Boucher RC, Harden TK. Release of cellular UDP-glucose as a potential extracellular signaling molecule. *Mol Pharmacol*. 2003;63(5):1190–1197.
55. Eigenbrodt E, Reinacher M, Scheefers-Borchel U, Scheefers H, Friis R. Double role for pyruvate kinase type M2 in the expansion of phosphometabolite pools found in tumor cells. *Crit Rev Oncog*. 1992; 3(1–2):91–115.
56. Brautigam VM, Dubyak GR, Crain JM, Watters JJ. The inflammatory effects of UDP-glucose in N9 microglia are not mediated by P2Y14 receptor activation. *Purinergic Signal*. 2008;4(1):73–78.
57. Scrivens M, Dickenson JM. Pharmacological effects mediated by UDP-glucose that are independent of P2Y14 receptor expression. *Pharmacol Res*. 2005;51(6):533–538.
58. Artegiani B, Calegari F. Age-related cognitive decline: can neural stem cells help us? *Aging (Albany NY)*. 2012;4(3):176–186.
59. Lin YJ, Seroude L, Benzer S. Extended life-span and stress resistance in the Drosophila mutant methuselah. *Science*. 1998;282(5390):943–946.
60. Cho J, et al. Ewing sarcoma gene Ews regulates hematopoietic stem cell senescence. *Blood*. 2011; 117(4):1156–1166.
61. Cho JS, Kook SH, Robinson AR, Niedernhofer LJ, Lee BC. Cell autonomous and nonautonomous mechanisms drive hematopoietic stem/progenitor cell loss in the absence of DNA repair. *Stem Cells*. 2013;31(3):511–525.